UCBNE-5116

Performance Assessment for Geologic Disposal of High-Level Radioactive Wastes

Summary for Previous Studies for Coupled Phenomena

FY2007 Annual Report
For
UCBNE-KAERI Collaboration

Joonhong Ahn
Department of Nuclear Engineering
University of California, Berkeley
Berkeley, CA 94720-1730

July 20, 2008

Joonhong Ahn
Principal Investigator of the project
Department of Nuclear Engineering
University of California
Berkeley, CA 94720
USA

ahn@nuc.berkeley.edu

Table of Contents

List of Figures

List of Tables:

I. Background and Objectives

The MDPSA (multi-dimensional probabilistic safety assessment) code for performance and safety assessment for geologic disposal of high-level radioactive wastes developed by Korea Atomic Energy Research Institute (KAERI hereafter) can handle the groundwater and radionuclide transport in a saturation porous/fractured medium. KAERI is planning to improve the existing code system by implementing effects of coupled phenomena among thermal, hydrological, mechanical, and chemical processes.

In this joint project between KAERI and Department of Nuclear Engineering, University of California at Berkeley (UCBNE hereafter), for the project term between July 1, 2007 and February 29, 2008, by focusing on the thermal effects, development of fundamental methodology and theories to predict the effects of decay-heat load on the groundwater flow and radionuclide transport have been carried out toward the eventual development of computer codes for the radionuclide transport with coupled phenomena.

The following schedule was set in the agreement:

- Literature survey for existing models and codes (1 month): July 2007
- Establishment of governing equations for groundwater flow in T-H coupled conditions (1.5 months): August – September 2007
- Establishment of governing equations for radionuclide migration in porous and fractured media under T-H coupled conditions (1.5 months): September – October 2007
- Analytical solutions for the problems (2 months): November – December 2007
- Preparation of final report (1-2 months): January – February 2008

II. Literature survey

For the objective of this study, space-time-dependent profiles for temperature, water (or gas) saturation in pores, and pore velocities of groundwater and air/gas mixture in the near-field around a waste canister are fundamental outputs we need to obtain. Literature survey was carried out to understand governing equations for energy, momentum, and mass of groundwater for porous and fractured media. Particularly, previous studies for abstracted, simplified cases, for which analytical solutions were derived, were sought.

We identified a couple of key literatures in this field.[1, 2, 3, 4] Reference 1 shows the most comprehensive and general mathematical formulations for mass and heat transport in geologic media. Reference 2 shows concise mathematical formulation for two-phase flow problems around a waste package with a simplified geometry. A formulation for a cylindrical geometry is shown below. Reference 3 focuses on radionuclide release from a canister in a porous medium with groundwater flow. A case that may be relevant to this project was discussed, where natural convection of groundwater occurs around a waste package due to heat emission from a waste package. Simplification was introduced to derive analytical solutions to the problem. Reference 4 is about the TOUGH2 code, which is considered to be de facto standard for this type of problems.

Mechanical effects should also be incorporated in the hydrology model because (1) swelling of the bentonite buffer is significant, which affects pore structure and permeability for water and gas, and (2) aperture of fractures in host rock would be affected by the stress. Preliminary mathematical formulation with Hydro-Mechanical (HM) coupling for bentonite swelling was studied previously experimentally by Swedish groups, such as R. Pusch, et al.[5, 6] T. Kanno, et al.[7]. Other studies include by OECD.[8] In these previous studies, the primary interests are bentonite swelling due to imbibition of water to bentonite and water flow. Recently, Borrelli, et al.[9] studied effects of radionuclide migration in swelling bentonite in a fracture. This can be considered as a preliminary coupling of radionuclide transport with HM modeling for the engineered barrier region.

III. Groundwater flow in T-H coupled conditions

III.1. Introduction

We consider a water-saturated repository with the engineered barrier configuration including a metal waste package, bentonite-buffer material, and near-field host rock, constructed in a crystalline rock, such as granite.

It is considered that the temperature in the bentonite buffer should be kept lower than the boiling temperature of water to maintain swelling capability of the bentonite. At a higher temperature, the principal mineral in the bentonite, such as smectite, will alter to less swelling minerals, such as illite. Therefore, the waste package needs to be stored before emplacement in the repository until the heat emission from the package has become sufficiently low.

When the package is placed in a drift tunnel in the repository and the gap space between the package and the tunnel surface is backfilled and buffered with the bentonite, the bentonite is considered to be partially saturated with water. While the heat emission from the package is sufficiently low, there is still heat emission from the package at the time of emplacement. Thus, at early times, there is a partially saturated porous medium around the waste package. This unsaturated-ness will be kept for some time until the heat emission has become even lower and water in the surrounding near-field host rock infiltrates into the bentonite region. This infiltration will occur as a two-phase flow. Heat is coming from the package, through the buffer, and then dissipated into the surrounding rock. Water, on the other hand, comes from the near field rock into the bentonite, and eventually wets the surface of the waste package.

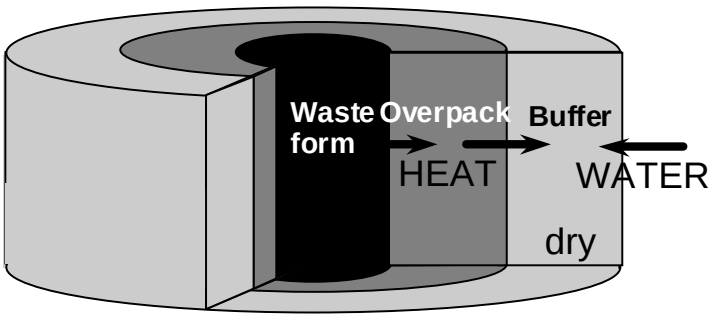

Figure 1: One-dimensional cylindrical geometry for the engineered barrier system.

The phenomena that would happen in this time interval would affect the “initial” conditions of the corrosion analysis for the waste package and of the radionuclide transport analysis after the package failure. Thus, *we identified that this time domain is crucially important for the reliability and fidelity of the repository performance assessment.*

Heat transfer in the vicinity of the waste package, where water saturation is the lowest in the bentonite buffer, is expected to be worse than in the vicinity of the buffer-rock interface. With water infiltration, which is driven mainly by capillary pressures, bentonite swells, resulting in evolution of pore structure. The heat conductivity and water permeability are strong functions of saturation, resulting in a non-linear, coupled problem including transfers of mass and energy. In the following formulation, we assume that the thermal equilibrium is established among the solid, liquid and gas phases in the bentonite.

In summary, by analyzing and formulating the aforementioned phenomena, we can answer such questions as:

- When will the bentonite region be re-wetted by groundwater?
- For how long will the metal canister be contacted by steam before water reaches the canister surface?

The information can be applied further to such analyses as:

- Metal canister corrosion (by steam and liquid water),
- Evolution of chemical conditions in the buffer after emplacement, and
- Evolution of mechanical conditions in the buffer after emplacement.

These can also be used to determine the conditions for radionuclide migration after the package failure, such as sorption distribution coefficients and solubilities for radionuclides.

III.2. Mathematical formulation

We consider mathematical formulation in a 1-D cylindrical coordinate system. For the unit control volume, we can write the following balance equations:

Mass conservation for water: $$\frac{\partial M_w}{\partial t}+\frac{1}{2\pi r}\frac{\partial Q_w}{\partial r}=0 \quad (1)$$

Mass conservation for air: $$\frac{\partial M_a}{\partial t}+\frac{1}{2\pi r}\frac{\partial Q_a}{\partial r}=0 \quad (2)$$

Energy conservation: $$\frac{\partial M_e}{\partial t}+\frac{1}{2\pi r}\frac{\partial Q_e}{\partial r}=0 \quad (3)$$

where

mass of water $M_w=\phi\left(S_\ell\rho_\ell X_\ell^w+S_g\rho_g X_g^w\right)$ [kg/m^3],

mass of air $M_a=\phi\left(S_\ell\rho_\ell X_\ell^a+S_g\rho_g X_g^a\right)$ [kg/m^3],

and, heat $M_a=\phi\left(S_\ell\rho_\ell u_\ell+S_g\rho_g u_g\right)+\left(1-\phi\right)c_r\rho_r T$ [J/m^3],

are formulated as shown above. Here, ϕ: the porosity of the buffer, S_ℓ and S_g: saturations, X_ℓ and X_g: mass fractions, ρ_ℓ and ρ_g the densities [kg/m^3], ρ_r the density of the bentonite, c_r the specific heat of bentonite [J/kg•K], u_ℓ and u_g the internal energy [J/kg], T temperature [^{o}C]. The subscripts *l* and *g* are gor the liquid and gas phases, respectively. Q is the flux flowing into the control volume. For the saturation and the mass fractions, the following relationship hold:

$$S_\ell + S_g = 1, \tag{4}$$

$$X_\ell^a + X_\ell^w = 1, \tag{5}$$

and

$$X_g^a + X_g^w = 1. \tag{6}$$

For the fluxes, by assuming the Darcy's law, we can write:

$$Q_w = -\frac{kk_{r\ell}X_\ell^w\rho_\ell}{\mu_\ell}2\pi r\frac{\partial P_\ell}{\partial r} + \left[-\frac{kk_{rg}X_g^w\rho_g}{\mu_g}2\pi r\frac{\partial P_g}{\partial r} - D_{va}\rho_g 2\pi r\frac{\partial X_g^w}{\partial r}\right], \tag{7}$$

$$Q_a = -\frac{kk_{r\ell}X_\ell^a\rho_\ell}{\mu_\ell}2\pi r\frac{\partial P_\ell}{\partial r} + \left[-\frac{kk_{rg}X_g^a\rho_g}{\mu_g}2\pi r\frac{\partial P_g}{\partial r} - D_{va}\rho_g 2\pi r\frac{\partial X_g^a}{\partial r}\right], \tag{8}$$

and

$$\begin{aligned} Q_a = &-h_\ell^a\frac{kk_{r\ell}X_\ell^a\rho_\ell}{\mu_\ell}2\pi r\frac{\partial P_\ell}{\partial r} + h_g^a\left[-\frac{kk_{rg}X_g^a\rho_g}{\mu_g}2\pi r\frac{\partial P_g}{\partial r} - D_{va}\rho_g 2\pi r\frac{\partial X_g^a}{\partial r}\right] \\ &-h_\ell^w\frac{kk_{r\ell}X_\ell^w\rho_\ell}{\mu_\ell}2\pi r\frac{\partial P_\ell}{\partial r} + h_g^w\left[-\frac{kk_{rg}X_g^w\rho_g}{\mu_g}2\pi r\frac{\partial P_g}{\partial r} - D_{va}\rho_g 2\pi r\frac{\partial X_g^w}{\partial r}\right] \\ &-\kappa(2\pi r)\frac{\partial T}{\partial r}, \end{aligned} \tag{9}$$

where k is the permeability [m^2] for water-saturated bentonite, $k_{r\ell}$ and k_{rg} the relative permeability, μ_ℓ and μ_g the viscosity [Pa s], P_ℓ and P_g the pressure, κ the heat conductivity [W/m•K], and h_ℓ and h_g the enthalpy [J/kg]. D_{va} is the diffusion coefficient [m^2/s].

Between the pressures, the relation

$$P_\ell = P_g + P_c, \tag{10}$$

is written, where P_c is the capillary pressure [Pa]. The gas-phase pressure is written as

$$P_g = P_v + P_a, \tag{11}$$

where P_v is the vapor pressure [Pa] and P_a is the partial pressure of the air [Pa]. Between the air partial pressure and the mole fraction of the air dissolved in water, Henry's law applies:

$$P_a = K_H X_\ell^a \frac{M_{water}}{M_{air}}. \tag{12}$$

For the vapor pressure, by Kelvin's law,

$$P_v(T, S_g) = P_{sat}(T) \exp\left\{\frac{P_c(S_g)}{\rho_\ell RT}\right\}, \tag{13}$$

where $P_{sat}(T)$ is the saturated vapor pressure at temperature *T*. The air partial pressure can be written by assuming an ideal gas as

$$P_a = \frac{RT}{M_{air}} \rho_g X_g^a. \tag{14}$$

In the aforementioned equation system, there are 14 unknown quantities: Q_w, Q_a, Q_e, S_ℓ, S_g, X_ℓ^w, X_ℓ^a, X_g^w, X_g^a, P_ℓ, P_g, P_a, P_v, and *T*. For these there are 14 independent equations as labeled in the above.

Within those parameters introduced so far, ρ_ℓ, ρ_g, u_ℓ, u_g, h_ℓ, h_g, μ_ℓ and μ_g can be formulated by the state variables P_ℓ, P_g, and *T*. The heat conductivity κ is a function of water saturation S_ℓ given as

$$\kappa = \kappa_g + \sqrt{S_\ell}\left(\kappa_\ell - \kappa_g\right),$$

where κ_ℓ and κ_g are the conductivity with full saturation with water or air, respectively.

The capillary pressure P_c, the relative permeability $k_{r\ell}$ and k_{rg} are functions of saturation. Various different functions were proposed. For example,[10] Figure 2 depicts the following formulas:

Capillary pressure: $$P_c(S_\ell) = \begin{cases} 0, & S_\ell \geq S_{\ell s} \\ -P_o\left(S_{EF}^{-1/\lambda} - 1\right)^{1-\lambda}, & \\ -P_{\max}, & P_o\left(S_{EF}^{-1/\lambda} - 1\right)^{1-\lambda} \geq P_{\max} \end{cases} \quad (15)$$

Relative permeability: $$k_{r\ell}(S_\ell) = \begin{cases} \sqrt{S_{EF}}\left[1-\left(1-S_{EF}^{1/\lambda}\right)^{\lambda}\right], & S_\ell \leq S_{\ell s} \\ 1, & S_\ell \geq S_{\ell s} \end{cases} \quad (16)$$

$$k_{rg}(S_\ell) = 1 - k_{r\ell}(S_\ell)$$

where $$S_{EF} = \frac{S_\ell - S_{\ell r}}{S_{\ell s} - S_{\ell r}}.$$

This function implies that infiltration of water is assumed to be difficult at a small relative permeability for water. With the liquid saturation greater than 90%, significant water infiltration is assumed. $S_{\ell r}$ is the liquid saturation, below which the liquid phase in the pores is not continuous anymore, so that the pressure does not transmit through the liquid phase.

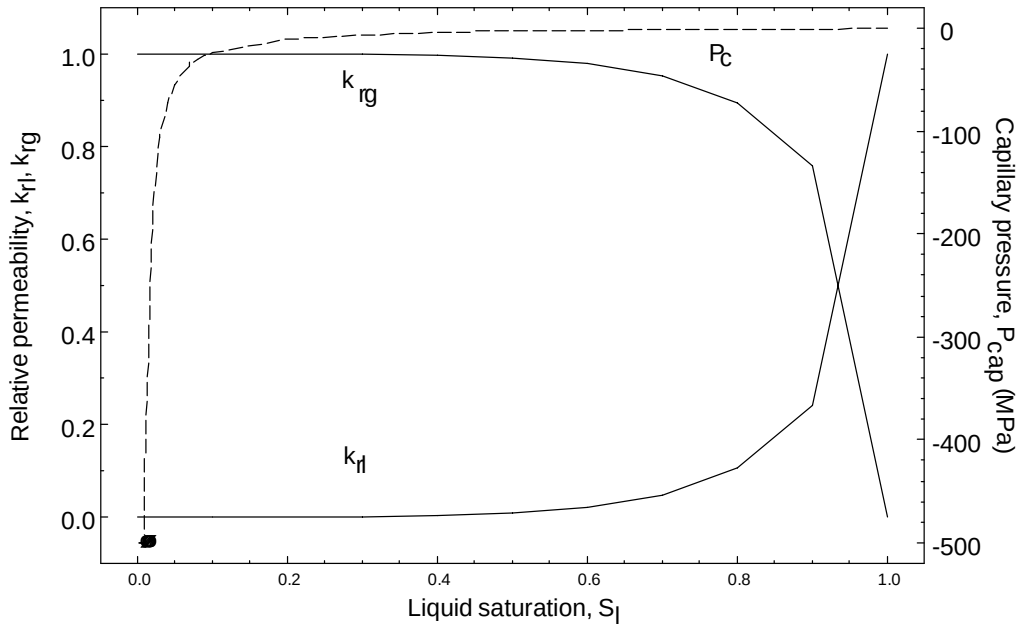

Figure 2: Assumed functions for relative permeability and capillary pressure

III.3. Parameter values and numerical results

For solving the above problem, we need to determine the initial and boundary conditions. For the system depicted in Figure 1, we consider the following situation, for example. At t = 0, in the whole bentonite region, some initial values are assumed for air partial pressure, vapor pressure, temperature, and gas saturation. The host rock surrounding the bentonite is assumed to be saturated with water all the time. At the package/bentonite interface, mass fluxes are zero. The heat flux from the waste package will be a known function of time. For this, we can write the side conditions as follow:

Initial conditions:

$P_a = P_{a0},\ P_v = P_{v0},\ T = T_0,\ S_g = S_{g0}$ in the whole bentonite region,

$T = T_0,\ S_g = 0$ in the surrounding rock,

Boundary conditions:

$Q_a = 0,\ Q_w = 0,\ Q_e = 2\pi q(t),$ at the interface between the bentonite and the package

$S_g = 0$ at the interface between the bentonite and the rock.

The decay heat function $q(t)$ is given in Figure 3. It is assumed that the waste canister includes radionuclides from PWR spent fuel reprocessing with 4 year cooling time before reprocessing and 30 year fooling time as a waste glass before emplacement in the repository. Other parameter values are summarized in Table 1.

Figure 4 shows the profiles of the temperature and the gas saturation at the overpack/bentonite interface as a function of time. Two sets of results are shown. One set has been obtained by assuming the formulas given by (15) and (16). For the second set, a linear relationship between the relative permeability and the saturation is assumed while the same (15) is assumed for the capillary pressure. In either case, the temperature is below 100^{o}C all the time with the peak at a few years. Within a few hundred years, the temperature has come down to the ambient temperature. Observing the gas saturation profile, one can find that it will take a few decades for the overpack surface to be fully wetted. If we assume the formula (16) for the relative permeability, which is highly non-linear, the water flow from the outer boundary of the buffer is like a plug flow.

Figure 5 shows the spatial distributions of the temperature, gas and water saturations in the buffer at 1 year and 36 years. At one year, water infiltration has occurred in the 5-cm layer from the outer boundary. At 36 years, water has infiltrated through the buffer and the overpack surface is wetted nearly completely.

Table 1: Parameter Values Assumed for the Heat Analysis

Parameter	Notation	Value
Porosity	ε	0.3
Density of rock	ρ_r	2,000 kg/m^3
Heat conductivity at water saturation	κ_ℓ	2.0 W/m^{o}C
Heat conductivity at air saturation	κ_g	1.0 W/m^{o}C
Specific heat	c_r	1,130 J/kg^{o}C
Permeability	k	10^{-20} m^2
Initial temperature	T_0	30^{o}C
Initial air saturation	S_{g0}	0.8
Initial air pressure	P	10^5 Pa = 1 atm
Capillary pressure	λ	0.45
	$S_{\ell r}$	9.6E-4
	$S_{\ell s}$	1.0
	P_o	1.393 MPa
	P_{max}	500 MPa

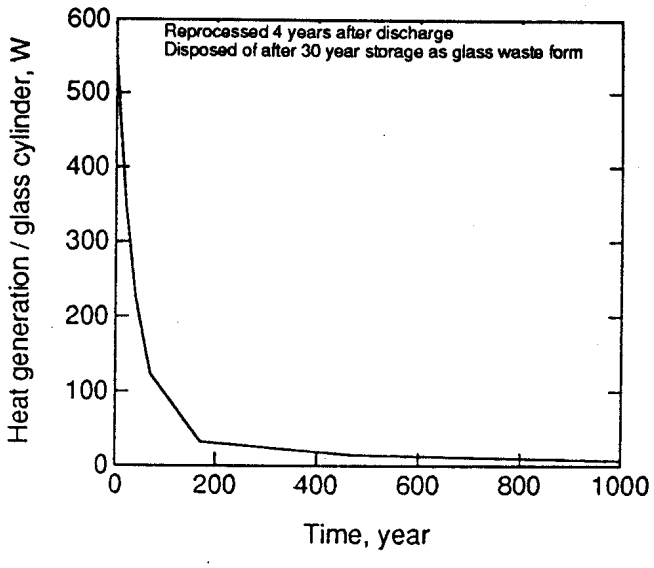

Figure 3: Decay heat profile assumed for the waste canister.

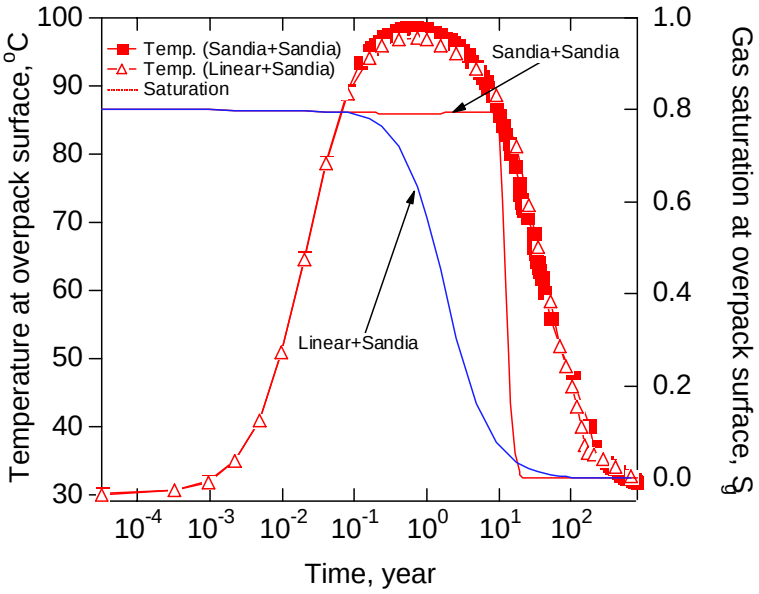

Figure 4: Time changes in temperature and moisture at the canister surface

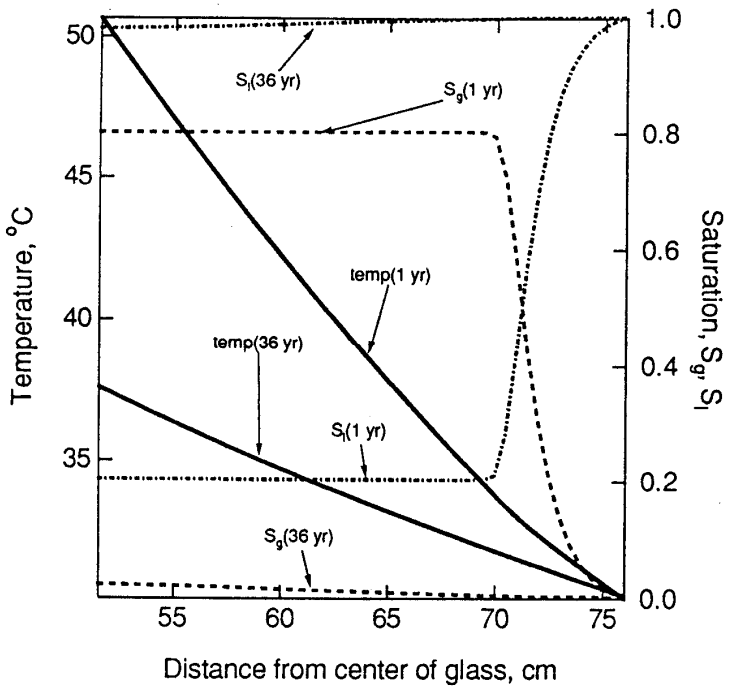

Figure 5: Spatial distributions of temperature and saturations in the buffer.

IV. Radionuclide migration in T-H-M-C coupled conditions

IV.1. Overview

Basic information necessary for analyses of radionuclide migration is space-time-dependent profiles for water (or gas) saturation, and physico-chemical reactions of radionuclides with other chemical species, especially with the solid phases of the host rock and buffer materials in the EBS.

Preliminary analyses with T-H coupling revealed that direct effects of heat emission on radionuclide migration would be secondary. This is because waste packages will be placed in the repository only after the heat emission from packages are sufficiently decreased due to temperature limitation with the bentonite material. Furthermore, considering a long time before package failure, the temperature would become even lower by the time the package fails and radionuclide release to the bentonite begins. It is considered that the package failure time is designed to be at minimum 1,000 years, likely to be longer than a few thousands to 10,000 years. So, in a nominal scenario, when radionuclide release starts, the temperature around the waste package is considered to be back at the ambient temperature.

In an accidental scenario, where packages fail early while still heat emission is significant, water density in surrounding host rock will be affected, resulting in an enhanced water flow around the waste package. Effects of free convection on radionuclide release from the waste package was first formulated by Chambré, et al. (see Ref. 3). A brief summary and discussions are given in Section IV.2.

A potentially important scenario is bentonite degradation due to an elevated temperature before the package failure. The following T-H-C coupling is observed. In groundwater, potassium ion is usually observed. It will alter smectite into illite. The reaction speed will be greater for higher temperature. The permeability will increase over the time, resulting in faster mass transfer within the engineered-barrier region. The problem of bentonite degradation due to illitization reaction with potassium ion was first formulated by Ahn.[11] It was observed that adverse effects of illitization were significant only when the bentonite temperature is as high as 90 degree C. A summary and discussions are given in Section IV.3.

An example for a coupling of H-M-C is bentonite extrusion in fractures in the host rock. Bentonite swells by imbibing water. The swelling pressure results from the electrical double layers between plate-like bentonite particles, and is dependent on cation concentrations in the water phase. Due to the electric repulsive force between bentonite particles, negative pressure is created, and water is sucked into the bentonite region, and in return, the volume of the bentonite region increases. Swelling of bentonite was studied experimentally and theoretically by several researchers in various different conditions and assumption. Borrelli and Ahn (Ref. 9) first studied the effects of bentonite swelling on the

radionuclide migration. Their studies revealed that sorption of radionuclides on moving bentonite particles in a planar fracture plays an important role. With sorption stronger than a certain threshold level, radionuclides would be confined within the bentonite extrusion region in a planar fracture. Their studies, however, did not include effects of temperature, or effects of cation concentrations on swelling. Summary is given in Section IV.4.

IV.2. Radionuclide Release by Diffusion and Free Convection

The problem concerns the mass transfer from a heated vertical cylinder which is embedded in a water-saturated porous medium. The temperature of the cylinder exceeds that of the surrounding with a result that a free convection pattern develops which drives the fluid along the cylinder surface. This induced velocity affects the mass transport of a diffusing species from the cylinder surface into the surrounding medium. The effects of free convection might be important during that time when the canister generates a sufficiently large amount of decay heat to maintain a temperature difference of about 50^{o}C or more between the canister surface and surrounding medium. The aim of the analysis is to determine the velocity, temperature, and concentration fields and to develop a formula for the surface mass flux.

The following assumptions are made:

- A steady state description is adopted.
- The vertical cylinder surface is replaced by a flat plate surface having the same length as the cylinder and a width equal to the cylinder circumference.
- The pore water is assumed to have temperature independent properties except for its density. The water flow obeys Darcy's law. The fluid filling the porous medium is assumed to be a single phase.
- Boundary layer theory simplifications are assumed valid.

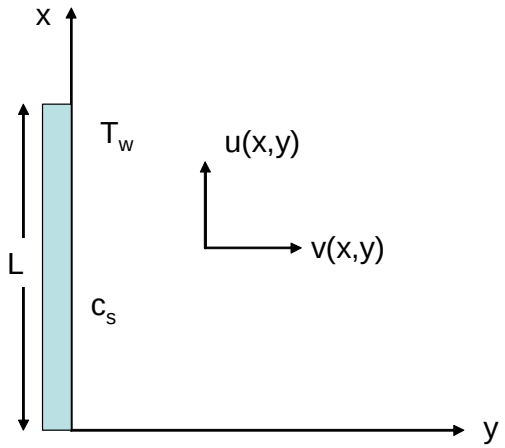

Figure 6: Coordinate system used in the free convection model.

The governing equations are:

Conservation of mass: $$\frac{\partial u}{\partial x}+\frac{\partial v}{\partial y}=0\,, \tag{17}$$

Conservation of momentum: $$u\left(x,y\right)=-\frac{k}{\mu}\left(\frac{\partial p}{\partial x}+\rho g\right), \tag{18}$$

$$v\left(x,y\right)=-\frac{k}{\mu}\frac{\partial p}{\partial y}\,, \tag{19}$$

Conservation of energy: $$u\frac{\partial T}{\partial x}+v\frac{\partial T}{\partial y}=\alpha_e\nabla^2 T\,,\ \ \alpha_e\equiv\frac{\lambda_e}{\rho c_p}\,, \tag{20}$$

Conservation of species: $$u\frac{\partial \hat{c}}{\partial x}+v\frac{\partial \hat{c}}{\partial y}=\varepsilon D_f\nabla^2\hat{c}\,, \tag{21}$$

Equation of state of liquid: $$\rho=\rho_\infty\left\{1-\beta\exp\left(T-T_\infty\right)\right\}, \tag{22}$$

where $$\nabla^2\equiv\frac{\partial^2}{\partial x^2}+\frac{\partial^2}{\partial y^2}\,. \tag{23}$$

The coordinate system is shown in Figure 6. The velocity components *u* and *v* point respectively into the *x* and *y* directions. In the above equations, *p*, *T*, ρ, c_p are the pressure, temperature, density and heat capacity of the liquid and ρ_∞ its density far away from the plate. *k* is the permeability. λ_e is the effective thermal conduction of water-saturated medium. μ and β are dynamic viscosity and coefficient of thermal expansion of the liquid in the porous medium, respectively. D_f is the diffusion coefficient of the diffusing species in the liquid.

The boundary conditions are:

$$v\left(x,0\right)=0\,,\ \ T\left(x,0\right)=T_w\,,\ \ \hat{c}\left(x,0\right)=c_s\,,\ x>0, \tag{24}$$

$$u\left(x,\infty\right)=v\left(x,\infty\right)=0\,,\ \ T\left(x,\infty\right)=T_\infty\,,\ \ \hat{c}\left(x,\infty\right)=0\,,\ x>0. \tag{25}$$

There will be a “slip” condition for the *u* component of the velocity at the plate surface which is as yet unknown. Furthermore, the temperature difference T_w-T_∞ which depends among other parameters on the heat release from the cylinder is also determined subsequently.

Equation (17) can be satisfied by introducing the stream function $\psi(x,y)$ with

$$u(x,y)=\frac{\partial\psi}{\partial y},\quad v(x,y)=-\frac{\partial\psi}{\partial x}. \tag{26}$$

If one differentiates (18) with respect to *y*, (19) with respect to *x* and then algebraically adds the resulting equations, one obtains with help of (22) and (26),

$$\left(\frac{k}{\mu}\rho_\infty\beta g\right)\frac{\partial T}{\partial y}=\nabla^2\psi. \tag{27}$$

On the other hand, (20) and (21), expressed with (26), give

$$\frac{\partial\psi}{\partial y}\frac{\partial T}{\partial x}-\frac{\partial\psi}{\partial x}\frac{\partial T}{\partial y}=\alpha_e\nabla^2 T, \tag{28}$$

and

$$\frac{\partial\psi}{\partial y}\frac{\partial\hat{c}}{\partial x}-\frac{\partial\psi}{\partial x}\frac{\partial\hat{c}}{\partial y}=\varepsilon D_f\nabla^2\hat{c}. \tag{29}$$

One has thus these three governing equations for the determination of the unknown functions ψ, *T*, and $\hat{c}$. For the purpose of establishing the main physical features of the solution, it is convenient to utilize the boundary layer simplifications. These imply that the transport of mass, energy and concentration in the major flow direction (i.e., *u*) is small compared to that normal to the plate. With

$$\frac{\partial^2\psi}{\partial x^2}\ll\frac{\partial^2\psi}{\partial y^2},\quad \frac{\partial^2 T}{\partial x^2}\ll\frac{\partial^2 T}{\partial y^2},\quad \frac{\partial^2\hat{c}}{\partial x^2}\ll\frac{\partial^2\hat{c}}{\partial y^2}. \tag{30}$$

Equations (27), (28) and (29) result in

$$\left(\frac{k}{\mu}\rho_\infty\beta g\right)\frac{\partial T}{\partial y}=\frac{\partial^2\psi}{\partial y^2}. \tag{31}$$

$$\frac{\partial\psi}{\partial y}\frac{\partial T}{\partial x}-\frac{\partial\psi}{\partial x}\frac{\partial T}{\partial y}=\alpha_e\frac{\partial^2 T}{\partial y^2}, \tag{32}$$

and

$$\frac{\partial\psi}{\partial y}\frac{\partial\hat{c}}{\partial x}-\frac{\partial\psi}{\partial x}\frac{\partial\hat{c}}{\partial y}=\varepsilon D_f\frac{\partial^2\hat{c}}{\partial y^2}. \tag{33}$$

These equations are subject to the boundary conditions

$$\frac{\partial \psi}{\partial x}(x,0)=0\,,\quad T(x,0)=T_w\,,\quad \hat{c}(x,0)=c_s\,,\ x>0, \tag{34}$$

$$\frac{\partial \psi}{\partial x}(x,\infty)=\frac{\partial \psi}{\partial y}(x,\infty)=0\,,\quad T(x,\infty)=T_\infty\,,\quad \hat{c}(x,\infty)=0\,,\ x>0. \tag{35}$$

Equations (31) and (32), which are coupled equations for T and ψ, are solved first. One determines thereby the temperature induced stream function $\psi(x,y)$ which describes the free convection flow pattern. With knowledge of ψ, one can then solve for the concentration $\hat{c}(x,y)$ separately. For this reason, we concentrate first on the solution of (31) and (32). These partial differential equations are reduced to ordinary differential equation by the introduction of the similarity variables

$$\eta = Ra^{1/2}\frac{y}{\sqrt{xL}}\,, \tag{36}$$

$$\psi = \alpha_e Ra^{1/2}\sqrt{\frac{x}{L}}f(\eta)\,, \tag{37}$$

$$\theta(\eta)=\frac{T-T_\infty}{T_w-T_\infty}\,, \tag{38}$$

$$c(\eta)=\frac{\hat{c}}{c_s}\,, \tag{39}$$

where

$$Ra=\frac{\rho_\infty g}{\alpha_e}\left(\frac{k}{\mu}\right)\beta(T_w-T_\infty)L\,. \tag{40}$$

Here L is the length of the plate and Ra is the Rayleigh number of the liquid-saturated porous medium. With these variables the governing equations reduce to

$$f''(\eta)-\theta'(\eta)=0\,, \tag{41}$$

$$\theta''(\eta)+\frac{1}{2}f(\eta)\theta'(\eta)=0\,, \tag{42}$$

$$\frac{1}{\Lambda}c''(\eta)+\frac{1}{2}f(\eta)c'(\eta)=0\,, \tag{43}$$

where $$\Lambda = \frac{\alpha_e}{\varepsilon D_f} = Le \tag{44}$$

is the Lewis number. As can be seen by introducing the new variables into (34) and (35), the boundary conditions transform to

$$f(0) = 0, \;\; \theta(0) = 1, \;\; c(0) = 1, \tag{45}$$

$$f'(\infty) = 0, \;\; \theta(\infty) = 0, \;\; c(\infty) = 0. \tag{46}$$

A final integral of (41), which satisfies the boundary conditions (46), is given by

$$f'(\eta) = \theta(\eta). \tag{47}$$

Since the *x* component of the free convection velocity is determined by

$$u = \frac{\partial \psi}{\partial y} = \left(\frac{\alpha_e}{L} Ra \right) f'(\eta), \tag{48}$$

one observes that the normalized vertical velocity $\dfrac{u}{\left(\dfrac{\alpha_e}{L} Ra \right)}$ and the temperature distribution $\theta(\eta)$ are of the same form, according to (47). Thus, the determination of the function $f(\eta)$ is of central importance. To obtain an equation for $f(\eta)$, eliminate $\theta(\eta)$ between equations (41), (42) and (43), with the result that

$$\frac{d^3 f}{d\eta^3} + \frac{1}{2} f(\eta) \frac{d^2 f}{d\eta^2} = 0. \tag{49}$$

Exactly the same differential equation arises in the problem of the boundary layer flow of a viscous fluid over a flat plate, the famous Blasius problem. But in contrast to the boundary conditions $f(0) = f'(0) = 0, \;\; f'(\infty) = 1$ in that problem, the conditions for the present case read

$$f(0) = 0, f'(0) = 1, \;\; f'(\infty) = 0. \tag{50}$$

The qualitative shape of the solution $f(\eta)$ of (49), (50) and that of its derivative $f'(\eta)$ are shown in Figure 7. As already stated, the free convection induced vertical velocity

component and the temperature distribution normal to the plate are both characterized by the shape of the $f'(\eta)$ function.

Next we determine the mass transfer from the vertical surface. For this one requires the normal derivative $\left.\frac{\partial \hat{c}}{\partial y}\right|_{y=0}$ which in turn involves $\left.\frac{\partial c}{\partial \eta}\right|_{\eta=0}$. But, η contains *Ra* and in this Rayleigh number there occurs the as yet unknown temperature difference $(T_w - T_\infty)$. $(T_w - T_\infty)$ is determined by heat flux through the canister surface and the convective and conductive heat transport into the porous medium. So, one must first find $(T_w - T_\infty)$. The local heat transfer from the surface of the plate is defined by

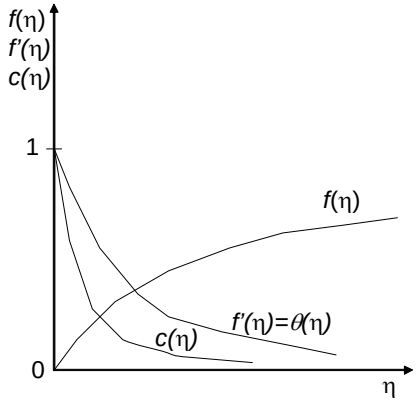

Figure 7: Qualitative shapes of functions for large Lewis number.

$$q'' = -\lambda_e \left.\frac{\partial T}{\partial y}\right|_{y=0}, \tag{51}$$

which with (36) and (38) yields

$$q'' = -\lambda_e (T_w - T_\infty)^{3/2} \left(\frac{\rho_\infty \beta g}{\alpha_e}\frac{k}{\mu}\right)^{1/2} x^{-1/2}\theta'(0). \tag{52}$$

The total rate of heat transfer from a plate of length *L* and width *W* is then

$$Q = W\int_0^L q''(x)\,dx = -W\lambda_e (T_w - T_\infty)^{3/2} \left(\frac{\rho_\infty \beta g}{\alpha_e}\frac{k}{\mu}\right)^{1/2} 2L^{1/2}\theta'(0). \tag{53}$$

Figure 8 shows the variation of spent fuel heat generation with time.

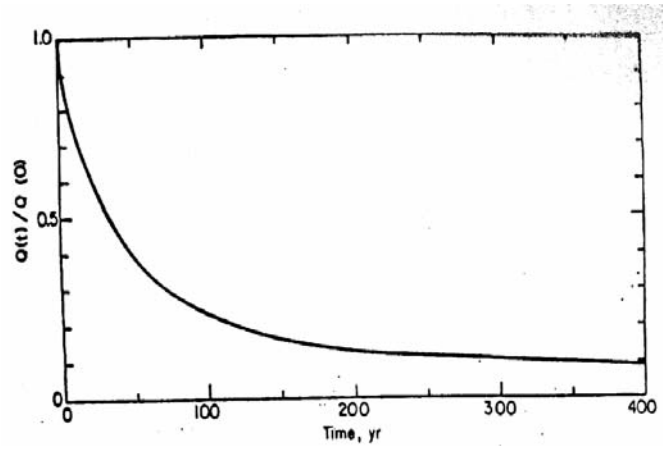

Figure 8: Variation of normalized decay heat generation of a waste canister with time *Q*(0) as the initial decay heat generation equal to 550 W.

We now define the magnitude of the average heat flux from the entire plate as

$$\overline{q}'' \equiv \frac{|Q|}{WL} = \lambda_e \left(T_w - T_\infty\right)^{3/2} \left(4 \frac{\rho_\infty \beta g}{L \alpha_e} \frac{k}{\mu} \right)^{1/2} \left|\theta'(0)\right|. \tag{54}$$

Hence the desired temperature difference between the plate surface and the porous media is given by

$$\left(T_w - T_\infty\right) = \sqrt[3]{\frac{\left(\overline{q}''\right)^2}{\lambda_e^2 \left(4 \frac{\rho_\infty \beta g}{L \alpha_e} \frac{k}{\mu} \right) \left|\theta'(0)\right|^2}}. \tag{55}$$

$\left(T_w - T_\infty\right)$ is seen to be a function of the average heat flux issuing from the fuel canister and the properties of the porous medium. The assumption is made that the average heat flux varies so slowly with time so that (55) can be applied to a quasi-steady state. Figure 9 shows a typical trend for this temperature difference as a function of time for a given $\overline{q}''(t)$ descriptive of the waste in a canister. The temperature difference drops to 100°C in about 130 years if we use the parameter values shown in Table 2.

From (48) and (50), the free convection velocity component along the plate surface (slip velocity) is given by

$$u(x,0) = \left(\frac{\alpha_e}{L} Ra \right) f'(0) = \frac{\alpha_e}{L} Ra = \rho_\infty g \beta \left(\frac{k}{\mu} \right) \left(T_w - T_\infty\right). \tag{56}$$

For a temperature difference of 100°C, one computes u = 0.34 m/yr. This is competitive with commonly assumed and used groundwater velocity of 1 m/yr in the far-field calculations. Figure 9 gives the magnitude of the free convection velocity as a function of time.

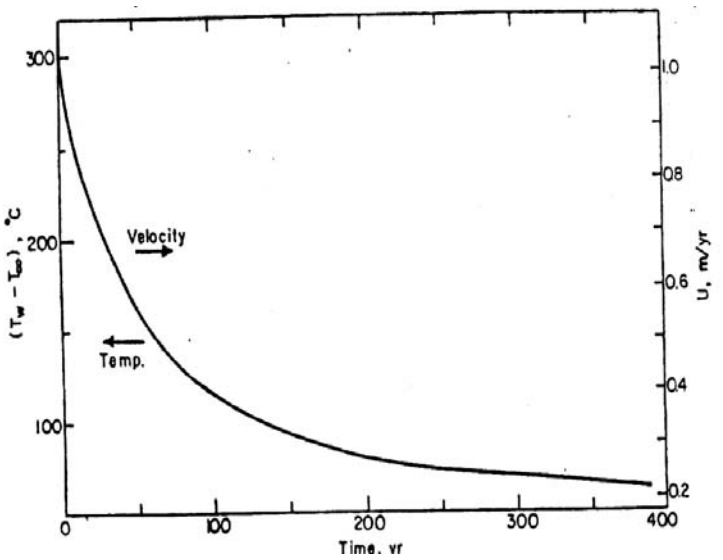

Figure 9: Variation of temperature difference and free convection velocity with time.

Table 2: Parameter Values Assumed for Numerical Evaluations

Thermal conductivity of the water-saturated porous media, λ_e	2.894 W/m°C	Ambient density of water, ρ_∞	1000 kg/m^3
Permeability, k	2.96E-14 m^2	Length of the cylinder, L	4.7 m
Dynamic viscosity of water, μ	5.5E-4 kg/m·s	Radius of the cylinder, r	0.178 m
Thermal expansion coefficient of water, β	2.07E-4 1/K	Initial total heat release rate, $Q(0)$	550 W
Heat capacity of water, c_p	4.184E3 J/kgK	The derivative of the normalized temperature at the surface, $\theta'(0)$	-1/π

The local mass transfer rate from the plate is now computed from the solution of (43) subject to the boundary conditions (45) and (46) for $c(\eta)$. The solution is

$$c(\eta) = 1 - \frac{I(\eta;\Lambda)}{I(\infty;\Lambda)}, \text{ where } I(\eta;\Lambda) = \int_0^{\eta} \exp\left(-\frac{\Lambda}{2}\int_0^{\eta'} f(s)\,ds\right) d\eta', \tag{57}$$

so that the surface mass flux is

$$\vec{j} = -D_f \varepsilon \left.\frac{\partial \hat{c}}{\partial y}\right|_{y=0} = -D_f \varepsilon c_s \left.\frac{\partial \eta}{\partial y}\frac{dc}{d\eta}\right|_{\eta=0}. \tag{58}$$

In view of (36) and (57),

$$\vec{j} = D_f \varepsilon c_s \left(\frac{Ra}{xL}\right)^{1/2} \frac{1}{I(\infty;\Lambda)}. \tag{59}$$

The definite integral $I(\infty;\Lambda)$ involves function $f(\eta)$,. i.e., the solution of (49). For complete evaluation of this integral for arbitrary value of the Lewis number, more mathematical procedures are involved. We develop here the asymptotic form of this integral for large values of Λ, which may arise due to small values of the diffusion coefficient in porous media. In this case the concentration boundary layer is very thin compared with the thermal layer, as sketched in Figure 7. One can then approximate $f(\eta)$ by the first order term of its power series expansion, i.e.,

$$f(\eta) = \eta + O(\eta^2). \tag{60}$$

If we neglect terms of $O(\eta^2)$,

$$I(\infty;\Lambda) = \int_0^{\infty} \exp\left(-\frac{\Lambda}{4}\eta^2\right) d\eta = \sqrt{\pi/\Lambda}, \text{ for } \Lambda \text{ large.} \tag{61}$$

Thus, (59) yields

$$\vec{j} = D_f \varepsilon c_s \left(\frac{\Lambda Ra}{xL\pi}\right)^{1/2}. \tag{62}$$

If one expresses *Ra* by (40) and Λ by (44),

$$\vec{j} = D_f \varepsilon c_s \left(\frac{1}{\pi}\frac{\rho_\infty g\beta}{\varepsilon D_f}\frac{k}{\mu}(T_w - T_\infty)\frac{1}{x}\right)^{1/2}. \tag{63}$$

IV.3. Effects of Buffer Degradation

Due to elevated temperature and presence of potassium ion in groundwater, smectite, the major mineral in the buffer, changes into illite. As the illite content in the buffer increases, hydraulic conductivity of the buffer will increase, while sorption capacity of the buffer will decrease.[12] Increase in hydraulic conductivity enhances water flow in the engineered barriers, resulting in faster waste glass dissolution and faster radionuclide transport. Furthermore, decrease in sorption distribution coefficients with increasing illite content results in increase in mass release rates of radionuclides at the outer boundary of the engineered barriers.

In this section, first we assume time-dependent hydraulic conductivity and sorption distribution coefficients by linear interpolation as the illite content changes with time. Then, models are established for (1) groundwater flow in the engineered barriers, (2) waste glass dissolution, and (3) mass transport through the buffer. Mass release rates of Am and Np at the outer boundary of the buffer are evaluated numerically, and effects of smectite illitization on the performance of the engineered barriers are shown quantitatively.

Here, we utilize the results by Altaner.[13] He estimated values of a potassium diffusion coefficient, smectite illitization reaction rate constant, and a Darcy velocity in a bentonite layer by interpreting zoned K-bentonite with illite-rich contacts and smectite-rich interiors as products of potassium metasomatism. He established a mathematical model of K+ transport, assuming the smectite illitization as

$$K^+ + \text{X-Smectite} \rightarrow \text{I/S} + \text{Quartz} + X^+, \tag{64}$$

where X^+ is an exchangeable cation such as Na^+ or Ca^{2+} included in smectite, I/S mixed-layer illite/smectite. He reported that potassium diffusion coefficient is in the order of 10^{-7} cm^2/sec and that the reaction rate constant varies from 10^{-15} sec^{-1} (50°C) to 10^{-10} sec^{-1} (150°C).

The mathematical model for potassium transport and smectite illitization is given in Ref. 13 and cited here:

$$\frac{\partial C_K}{\partial t} = D_K \frac{\partial^2 C_K}{\partial x^2} - W\left(C_{sm}\right)^{\alpha}\left(\frac{C_K}{C_{K0}}\right), \quad \frac{dC_{sm}}{dt} = -k\left(C_{sm}\right)^{\alpha}\left(\frac{C_K}{C_{Na}}\right)^{\beta}\left(\frac{C_K}{C_{K0}}\right),$$

$$0 < x < L,\ t > 0 \tag{65a, b}$$

We solve the above equations subject to the following side conditions:

$$C_K\left(x,0\right) = C_{K0}, \quad C_{sm}\left(0;x\right) = 1,\ 0 < x < L,$$

$$\left.\frac{\partial C_K}{\partial x}\right|_{x=0} = 0, \quad C_K(L,t) = 0, \; t > 0 \tag{66}$$

where C_K is the K^+ concentration in the pore water of the buffer [ppm], D_K the diffusion coefficient, C_{sm} the smectite ratio in the buffer [wt%], C_{K0} the boundary concentration of potassium, L the thickness of the buffer [cm], x the distance from the interface between the buffer and the inner engineered barrier, k the rate constant of smectite illitization, and

$$k = A\exp\left(-\frac{E}{RT}\right), \quad W = 4.53[\%\mathrm{K_2O}]\left(\frac{\rho_{\mathrm{sm}}}{\rho_W}\right)\left(\frac{1-\varepsilon}{\varepsilon}\right)\left(\frac{2AW_K}{AW_{K_2O}}\right)\left(\frac{10^6[\mathrm{ppm}]}{10^2[\mathrm{wt\%}]}\right)k\left(\frac{C_K}{C_{Na}}\right)^{\beta}, \tag{67}$$

$$d\ln\left(\frac{C_K}{C_{Na}}\right) = -\left(\frac{\Delta H}{R}\right)d\left(\frac{1}{T}\right). \tag{68}$$

AW is the atomic weight of the species of interest. See Table 3 for nomenclature and values of the parameters used in the above equations.

Table 3: Parameter Values for Illitization Calculation

Parameter	Value
Illite reaction order, α	1
Illite reaction order, β	1
Buffer porosity, ε	0.3
Buffer density, ρ_{sm}	2.0 g/cm^3
Water porosity, ρ_w	1.0 g/cm^3
Frequency factor for illitization, A	83.0 min^{-1}
Activation energy for illitization, E	19.6 kcal/mol
C_{K0}	200 ppm
Buffer thickness, L	100 cm
Diffusion coefficient of K^+ ion, D_K	3.15 cm^2/yr
C_K/C_{Na}	0.089 (90°C)
	0.072 (60°C)
	0.055 (30°C)
Rate constant for illitization, k	6.874E-5 yr^{-1} (90°C)
	5.948E-6 yr^{-1} (60°C)
	3.171E-7 yr^{-1} (30°C)

Figure 10 shows the average smectite content in the buffer as a function of time. Numerical calculation was done by the finite difference method. The left figure shows that its spatial distribution is relatively flat. This results from the much slower illitization

reaction than potassium diffusion in the buffer. For 30°C, illitization is negligibly small. With Figure 10, parameters such as the hydraulic conductivity and the sorption distribution coefficients can be evaluated as functions of time. We apply the averaged smectite ratio shown in the right figure for the entire bentonite-buffer region homogeneously.

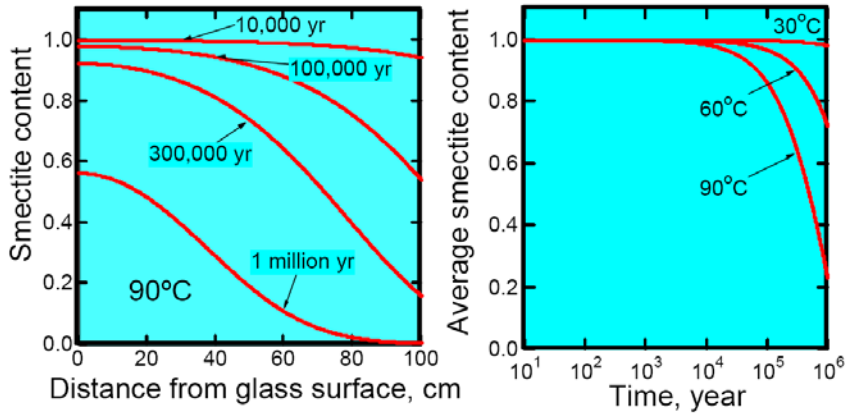

Figure 10: Spatial distributions of smectite content (mass fraction) in the buffer for four different time points at 90°C (left) and change of average smectite content in the buffer as a function of time for three different temperatures (right).

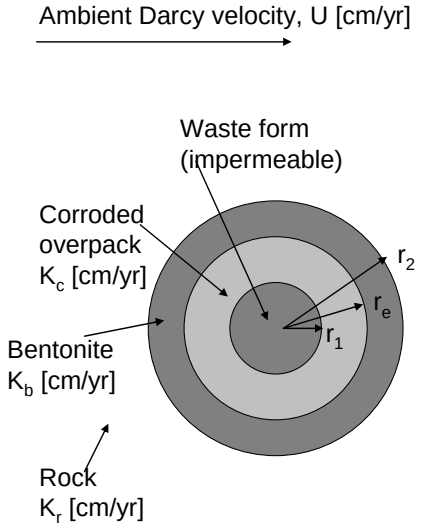

Figure 11: Three layers considered for evaluation of the water flow rate through the EBS

For water flow rate in the buffer, we assume that (1) the engineered barriers are approximated as a three-layer (waste glass, overpack, and buffer), infinitely long cylinder, (2) overpack has been corroded and can be treated as a uniform porous medium, (3) a steady

state flow velocity field is established at any time because illitization is very slow, and (4) porosities, densities, and hydraulic conductivity of corroded overpack and the host rock are constant. See Figure 11. By assumption (3), the flow potential ϕ can be obtained by solving the following governing equation,

$$r\frac{\partial}{\partial r}\left(r\frac{\partial \phi_i}{\partial r}\right)+\frac{\partial^2 \phi_i}{\partial \theta^2}=0, i=b,c,r\,, \tag{69}$$

Equation (69) can be written for the corroded overpack, the buffer, and the near-field rock. The boundary conditions can be set by considering continuity of potential and velocity at interfaces.

$$\left.\frac{\partial \phi_c}{\partial r}\right|_{r=r_1}=0,\quad 0\le\theta\le 2\pi\,,$$

$$K_c\left.\frac{\partial \phi_c}{\partial r}\right|_{r=r_e}=K_b\left.\frac{\partial \phi_b}{\partial r}\right|_{r=r_e},\quad \left.\frac{\partial \phi_c}{\partial \theta}\right|_{r=r_e}=\left.\frac{\partial \phi_b}{\partial \theta}\right|_{r=r_e},\quad 0\le\theta\le 2\pi\,,$$

$$K_b\left.\frac{\partial \phi_b}{\partial r}\right|_{r=r_2}=K_r\left.\frac{\partial \phi_r}{\partial r}\right|_{r=r_2},\quad \left.\frac{\partial \phi_b}{\partial \theta}\right|_{r=r_2}=\left.\frac{\partial \phi_r}{\partial \theta}\right|_{r=r_2},\quad 0\le\theta\le 2\pi\,,$$

$$-K_r\left.\frac{\partial \phi_r}{\partial r}\right|_{r\to\infty}=U\cos\theta\,,\quad 0\le\theta\le 2\pi\,.$$

Analytical solutions for the three-layer configuration can be obtained by extending the solution obtained by Chambré, et al.[14] for the two-layer configuration. Similarly, it can be expanded into the three-layer configuration as follow:

$$\phi_c\left(R,\theta\right)=-\frac{Ur_1}{k_r}A_c\left(R+\frac{1}{R}\right)\cos\theta,$$
$$\phi_b\left(R,\theta\right)=-\frac{Ur_1}{k_r}A_b\left(R+\frac{B_b}{R}\right)\cos\theta,$$
$$\phi_r\left(R,\theta\right)=-\frac{Ur_1}{k_r}\left(R+\frac{B_r}{R}\right)\cos\theta,$$

where $A_c=A_b\dfrac{2s_e^2}{s_e^2\left(\alpha_1+1\right)+\left(1-\alpha_1\right)}, A_b=\dfrac{2s_2^2}{s_2^2\left(\alpha_2+1\right)+\left(1-\alpha_2\right)B_b},,$

$$B_b = s_e^2 \frac{(\alpha_1+1)+(1-\alpha_1)s_e^2}{s_e^2(\alpha_1+1)+(1-\alpha_1)}, B_r = s_2^2 \frac{(1-\alpha_2)s_2^2+(\alpha_2+1)B_b}{s_2^2(\alpha_2+1)+(1-\alpha_2)B_b},$$

$$s_e = r_e/r_1, s_2 = r_2/r_1, \alpha_1 = K_c/K_b, \alpha_2 = K_b/K_r, R = r/r_1.$$

With this potential function, the Darcy velocity components in the radial and angular directions in each region can be evaluated by

$$u_j(r,\theta) = -K_j \frac{\partial \phi_j}{\partial r}, v_j(r,\theta) = -\frac{K_j}{r}\frac{\partial \phi_j}{\partial \theta}, j = c,b,r$$

The stream line function, $\psi(r,\theta)$, can be determined by the following relationships:

$$\frac{\partial \phi}{\partial r} = \frac{1}{r}\frac{\partial \psi}{\partial \theta}, \quad -\frac{\partial \psi}{\partial r} = \frac{1}{r}\frac{\partial \phi}{\partial \theta}$$

Therefore, we obtain

$$\psi_c(R,\theta) = -\frac{Ur_1}{k_r} A_c \left(R - \frac{1}{R}\right)\sin\theta,$$
$$\psi_b(R,\theta) = -\frac{Ur_1}{k_r} A_b \left(R - \frac{B_b}{R}\right)\sin\theta,$$
$$\psi_r(R,\theta) = -\frac{Ur_1}{k_r}\left(R - \frac{B_r}{R}\right)\sin\theta,$$

The stream line, which is tangent to the buffer/rock interface, represents the amount of flow that passes through the engineered barriers surrounding one-half of the waste glass. Thus, the amount of water that passes through the buffer per unit length of the waste glass cylinder, $Q(t)$, [cm^3/yr·cm] is then obtained as:

$$Q(t) = -2K_r \psi_r\left(s_2, \pi/2\right).$$

Or,
$$Q(t) = 4Ur_2 \frac{K_b(t)}{K_r} \frac{s_2^2 - B_b(t)}{s_2^2(\alpha_2(t)+1)+(1-\alpha_2(t))B_b}. \tag{70}$$

$K_b(t)$ is the hydraulic conductivity, expressed as:

$$K_b(t) = K_{sm} C_{sm}(t) + K_{il}\left[1 - C_{sm}(t)\right], \tag{71}$$

where K_{sm} and K_{il} are hydraulic conductivities of pure smectite and illite, respectively.

With (70) and the porosity of the buffer, ε, the height of the waste glass cylinder, H [cm], and the surface area of the waste glass, S [cm^2], the pore velocity in the pores of the buffer can be expressed as:

$$u_b(t) = \frac{Q(t)H}{\varepsilon S} \quad \text{[cm/yr]}. \tag{72}$$

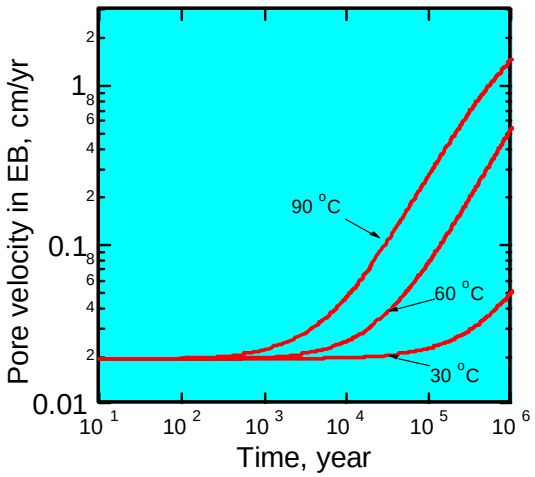

Figure 12: Pore velocity in the buffer region for three different temperatures.

Table 4: Parameter Values for Water Flow Calculation in the Buffer

Parameter	Value
Ambient Darcy velocity, U	100 cm/yr
Radius of the waste form, r_1	20 cm
Radius of the overpack, r_e	50 cm
Radius of the buffer, r_2	150 cm
Height of the canister, H	108 cm
Surface area of the EBS, S	14,000 cm^2
Hydraulic conductivity of the overpack, K_c	= K_b
Hydraulic conductivity of the rock, K_r	1E-6 cm/sec
Hydraulic conductivity of the buffer, $K_b(t)$	
K_{sm}	1E-11 cm/sec
K_{il}	1E-9 cm/sec
Porosity, ε	0.3

In Figure 12, $u_b(t)$ (72) is plotted, with the repository temperature as a parameter. With a higher temperature, illitization proceeds faster, and the hydraulic conductivity of the buffer becomes larger, resulting in greater pore velocity in the buffer. See Table 4 for parameter values used in the calculation. For the temperature as low as 30°C, the increase in pore velocity by illitization is negligibly small, whereas for 90°C, the pore velocity becomes almost two orders of magnitude greater than that of the initial value.

We consider two different glass dissolution mechanisms. The first one is the first-order chemical reaction, and the second one is alteration from the amorphous phase to more stable crystalline phase.[15] Rate of glass dissolution is determined by chemical reaction rate of dissolution and rate of mass transfer from the glass dissolution location by molecular diffusion and advection. Here, we adopt a simple one-dimensional planar geometry, and consider only waste glass and the buffer. We assume that the pore velocity in the buffer is homogeneous in the buffer, given by $u_b(t)$. Previous analyses show that glass dissolution reaction reaches a steady state in about 10 years. Because this is short enough for other time scales, we treat the pore velocity $u_b(t)$ as a constant, and solve the steady state equation (73).

Dissolved silica is transported by advection and molecular diffusion through the buffer pores. We neglect sorption of dissolved silica on the solid phase of the buffer, and time-dependency of porosity and density of the buffer. Then, the governing equation for the transport of dissolved silica is written as:

$$0 = D_s \frac{d^2C}{dx^2} - u_b \frac{dC}{dx}, 0 < x < L, \tag{73}$$

where C is the concentration of dissolved silica in pore water of the buffer, and D_s the diffusion coefficient of dissolved silica.

The boundary condition at the glass buffer interface can be set by balancing amount of mass coming in and coming out at the interface as follows:

$$\varepsilon\left[u_b(t)C(0;t) - D_s \left.\frac{dC}{dx}\right|_{x=0}\right] = j_o\left[1 - \frac{C(0;t)}{C^*}\right], t > 0, \tag{74}$$

$$C(L;t) = \bar{C}, t > 0, \tag{75}$$

where $\bar{C}$ is the background silica concentration in a groundwater, C^* the solubility of silica, and j_o the rate of glass matrix dissolution [g/cm^{2}yr].

For alteration, we assume a constant rate, j_{res} [g/cm^{2}yr]. With these, we can write the total glass dissolution rate $\mu_s(t)$ as:

$$\mu_s(t) = j_o\left[1 - \frac{C(0;t)}{C^*}\right] + j_{res}. \tag{76}$$

Thermodynamic data for parameters used in (76) are given by (3-24) to (3-28). For j_{res},

$$j_{res} = j_{res}^{90} \exp\left[\frac{A_{jres}}{\Re}\left(\frac{1}{363.15} - \frac{1}{T}\right)\right] \text{ [g/m}^2\text{-day]},$$

A_{jres} is 57.5 kJ/mol. j_{res}^{90} is 9.125E-5 g/cm^{2}day from Ref. 13.

Then, the total glass dissolution rate, $\mu_s(t)$, can be written analytically as

$$\mu_s(t) = j_o(1-\chi)\frac{(H-F)\tanh\left(Pe/2\right) + 1/2}{H\tanh\left(Pe/2\right) + 1/2} + j_{res}, \tag{77}$$

where $$Pe = \frac{u_b L}{D_s},\quad \chi = \frac{\bar{C}}{C^*},\quad H = \frac{1}{2} + \frac{j_o}{\varepsilon u_b C^*},\quad F = \frac{j_o}{\varepsilon u_b C^*} - \frac{\chi}{1-\chi}.$$

With (77), the inventory of waste glass is written as a function of time as:

$$M_s(t) = M_s^o - S\int_0^t \mu_s(\tau)\,d\tau, \tag{78}$$

where M_s^o is the initial inventory of waste glass. The leach time, T_L, is obtained by solving $M_s(T_L) = 0$.

Numerical results for (77) and (78) are shown in Figure 13. Although the pore velocity for 90°C becomes, during this time span, hundred fold greater, the total glass dissolution rate shows only 10 to 20% increase. This implies that molecular diffusion remains dominant to advective transport for the first several hundred thousand years. Notice that increase of the total glass dissolution rate becomes noticeable after all the waste glass has dissolved out. Therefore, for a practical purpose, smectite illitization has negligible effect on glass dissolution, and results of the previous analysis, where illitization is not taken into account, are found to be a very good approximation.

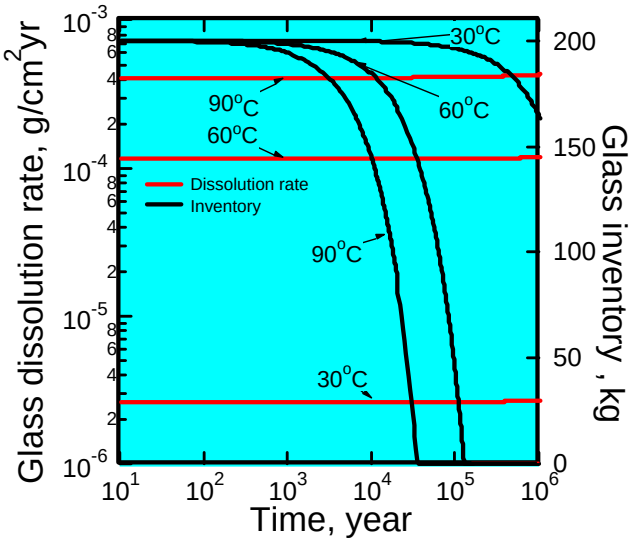

Figure 13: Glass dissolution rates and inventory for three different temperatures as functions of time.

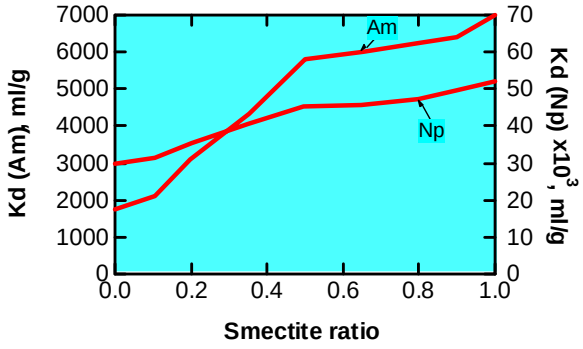

Figure 14: Sorption distribution coefficients for Am and Np with illite-smectite mixture as a function of the smectite ratio.[16]

The results of the experimental measurements for the sorption distribution coefficients for Am and Np with illite and smectite are plotted in Figure 14 as a function of smectite content. The sorption distribution coefficient on Kunigel V1 (100 % smectite) is shown. Qualitatively, the dependence of sorption distribution coefficient of Am on smectite content is very similar to that of Np(IV). While the sorption distribution coefficient does not change markedly with more than 50 % of smectite, it monotonously increases with the smectite content.

We consider transport of Am and Np through the buffer by considering that the composition of the buffer material changes with time. The governing equations for the Am isotopes are written as:

$$R_{Am}(t)\frac{\partial N_i}{\partial t} + N_i \frac{dR_{Am}(t)}{dt} + u_b(t)\frac{\partial N_i}{\partial x} = D_{Am}\frac{\partial^2 N_i}{\partial x^2} - \lambda_i R_{Am}(t) N_i,$$

$$0 < x < L,\ t > 0,\ i = 241,\ 243, \tag{79}$$

subject to the solubility-limited boundary conditions if Am precipitate exists at the glass dissolution location or the congruent release rate is assigned to the mass flux at the inner boundary $x = 0$. Note that the retardation factor is a function of time because the sorption distribution coefficient is due to the time-dependent illite fraction. For the solubility-limited boundary conditions, we need to assign a fraction of the solubility proportionally to the mass fraction of the isotope in the glass.

For ^{237}Np, we consider precipitation in the pores in the buffer due to radioactive decay of ^{241}Am. The model is the same as that shown in the previous study by Ahn and Suzuki.[17] Parameter values assumed are summarized in Table 5.

Table 5: Parameter values used for Am and Np transport in the buffer

Parameter	Value	Parameter	Value
Am solubility, N^*_{Am}	10^{-12} mol/cm^3	Np solubility, N^*_{Np}	10^{-15} mol/cm^3
Diffusion coefficient of Am in buffer, D_{Am}	315 cm^2/yr	Diffusion coefficient of Np in buffer, D_{Np}	315 cm^2/yr
Initial mass of ^{241}Am in a canister, M^o_{241}	0.291 mol	Decay constant of ^{237}Np, λ_{237}	3.24E-7 yr^{-1}
Initial mass of ^{243}Am in a canister, M^o_{243}	0.532 mol	Decay constant of ^{241}Am, λ_{241}	1.51E-3 yr^{-1}
		Decay constant of ^{243}Am, λ_{243}	8.72E-5 yr^{-1}

From Figure 15, for cases 60°C and 90°C, Am precipitate exists for 60 to 70 thousand years. Beyond this point, the boundary condition for Am transport in the buffer is given by the congruent release mode. For 30°C, no Am precipitate occurs because of low glass dissolution rates. The congruent release boundary condition is applied all the time at this low temperature.

Figure 16 depicts the movement of the Np precipitate front. The glass-buffer interface is located at 0. For 60°C and 90°C, the thickness of the precipitate region reaches about 9 cm from the surface of the glass, whereas for 30°C at most 2 cm.

Figure 17 shows the mass release rates of Am and Np from the outer surface of the buffer. At 60°C and 90°C, the ^{243}Am is released from the glass in the solubility-limited mode, whereas at 30°C it is released congruently with the glass dissolution. The release of ^{243}Am at 90°C is slightly greater after 100,000 years than that for 60°C. This is because at

90°C more smectite has been illitized and sorption retardation has become weaker. Release of ^{237}Np starts at around 400,000 years for 60°C and 90°C, which is earlier and greater than for 30°C because the precipitation front reaches farther from the glass surface.

From this analysis, the following can be concluded:

- Smectite illitization has negligible effects on glass alteration and radionuclide release from the waste glass. Although the pore velocity increases at most two orders of magnitude by illitization, molecular diffusion is still main transport mechanism.
- Decrease in sorption distribution coefficients has negligible effects on transport of Am because of relatively short half lives in comparison with slow illitization speed. Np transport is slightly enhanced by illitization.
- The key parameter in this analysis is the hydraulic conductivity of illite. With more reliable measurements for them, effects of illitization should be revisited.

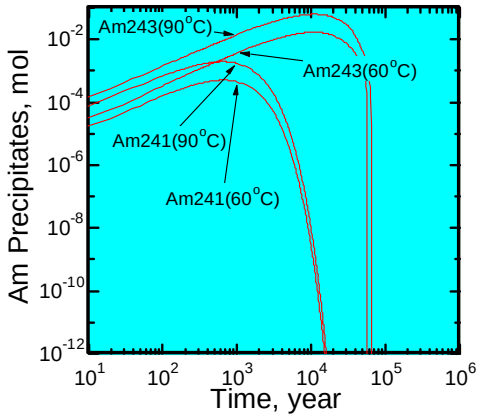

Figure 15: Americium precipitate generated at *x* = 0. No precipitate occurs for 30°C.

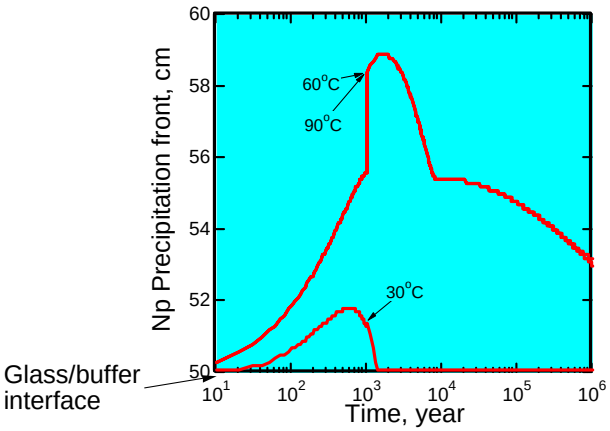

Figure 16: Movement of the front of Np precipitate in the buffer.

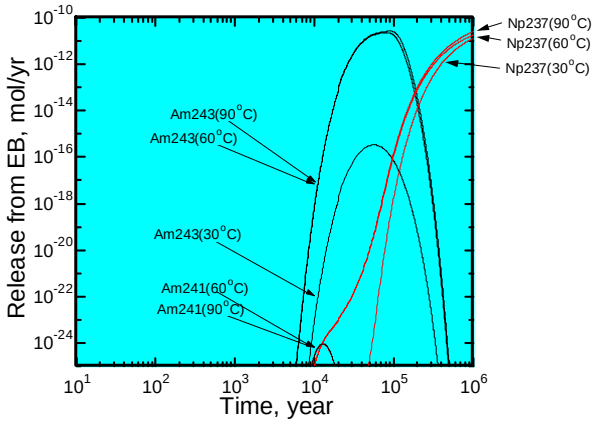

Figure 17: Release of Am and Np from the buffer. Release rates of ^{241}Am are too small to show in this scale.

IV.4. Effects of Buffer Swelling

In the engineered barrier system, (EBS), for a water-saturated repository, the function of the buffer is to inhibit the mass-transfer processes around the waste package. Compacted bentonite will be utilized for the buffer in the saturated repository primarily due to three favorable characteristics: low permeability, high sorption capacity, and high swelling capacity. Bentonite particles possess an overall negative charge and a high surface area and thus exhibit a high sorption capacity. Bentonite also swells greatly beyond its initial volume when in contact with water. This swelling effect results in extrusion of the buffer into the fracture, which can effectively seal the fracture and reduce releases of radionuclides.

The host rock containing fractures connecting the EBS to the far field represents an important domain. Due to the presence of fractures, infiltration of groundwater will form pathways for radionuclide release. Previous modeling studies of radionuclide transport in this region do not include effects of extruding bentonite on the transport of radionuclides. This paper presents a radionuclide migration model that considers the effects of bentonite extrusion by coupling an extrusion model with a radionuclide transport model. The bentonite extrusion changes temporally and spatially the fluid porosity in the fracture, resulting in variable hydraulic permeability and sorption retardation factors. In exchange with extruding bentonite, water comes into the bulk bentonite region.

The model space is defined in Figure 18. A planar fracture assumed to be initially filled with water intersects saturated bulk bentonite. The bulk bentonite is cylindrical; extrusion occurs in a radial direction as indicated. A constant radionuclide (N^*) source is located at the intersection between the bulk bentonite and the fracture (R_0). Conditions for this study assume that a sufficient amount of time has elapsed so that short lived radionuclides will have decayed; thus, considerations of heat emission and transfer, and temperature elevation, are neglected. Two distinct regions exist in the model space. One

region is defined by the extruding bentonite, and the other region exists beyond the expanding bentonite, containing only groundwater. The region of bentonite extrusion will also vary with time. Existence of bentonite particles beyond the tip in the form of colloidal suspension is neglected in the present model.

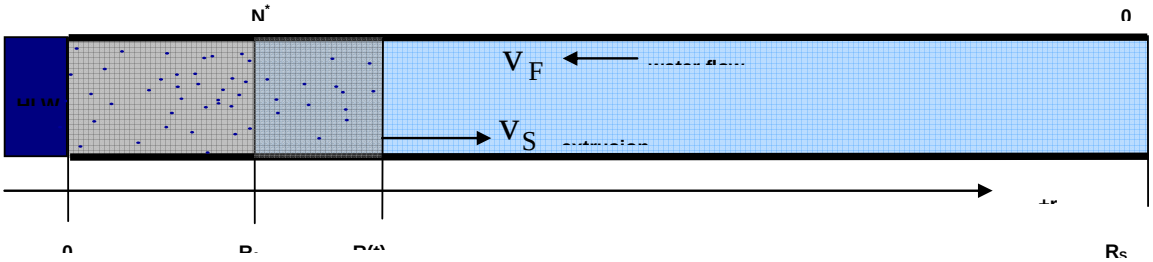

Figure 18: The model space for radionuclide transport modeling in extruding bentonite in a planar fracture.

The bentonite extrusion is modeled, based on transport of groundwater and characterized in terms of the void ratio (*e*), defined as the ratio of the void volume to the solid volume.[18],[19] Bentonite expands as a result of the electrical repulsive forces between the diffuse double layers of cations in the saturated system with the negatively charged, individual solid particles. Based on these forces, the distance between the particles increases, in order to achieve an equivalence of chemical potential; therefore, the bulk bentonite structure swells by dragging more water into it.

For a fixed volumetric element in fixed coordinates, the equations of continuity for water and solid material are provided, respectively, as[20]

$$\frac{1}{r}\frac{\partial}{\partial r}\left(r\gamma v_W \frac{e}{1+e}\right) = -\frac{\partial}{\partial t}\left(\gamma \frac{e}{1+e}\right), \quad t>0, \quad R_0 < r < R(t), \quad \text{for the water} \tag{80}$$

and

$$\frac{1}{r}\frac{\partial}{\partial r}\left(r v_S \frac{1}{1+e}\right) = -\frac{\partial}{\partial t}\left(\frac{1}{1+e}\right), \quad t>0, \quad R_0 < r < R(t), \quad \text{for the solid.} \tag{81}$$

The velocities v_W and v_S (*m/s*) correspond to water and solid, respectively. Both bentonite particles and water are assumed to be incompressible. The relative velocity is given by Darcy's law as

$$\frac{e}{1+e}(v_W - v_S) = -\frac{k}{\mu}\frac{\partial p}{\partial r}. \tag{82}$$

The parameters in (82) are permeability k (m^2), and water viscosity μ ($kg/m{\cdot}s$). With only considering horizontal fractures, (82) is expressed in terms of pore water pressure p

(N/m^2). The spatial and the time derivatives in (80) and in (81) are computed and added, then subtracted from the spatial derivative of Darcy's law. The results are substituted into the continuity equation for water (80) in order to obtain

$$\frac{1}{r}\frac{\partial}{\partial r}\left(\frac{k}{\mu}\frac{1}{1+e}\cdot r\frac{\partial p}{\partial r}\right)=\frac{1}{(1+e)^2}\frac{\partial e}{\partial t}. \tag{83}$$

By Terzaghi's one dimensional consolidation theory, the effective stress π' (N/m^2) is defined as $\pi' = \pi - p$.[21] The total stress π (N/m^2) acts on the entire area, which includes the soil skeleton and the voids and is assumed not to change with time. Therefore, changes in the effective stress and pore water pressure are related by

$$\frac{d\pi'}{dp} = -1. \tag{84}$$

The governing equation (83) can be modified by making use of the definition of the coefficient of compressibility a_V (m^2/N), and (84) as

$$\frac{\partial p}{\partial r}=\frac{\partial p}{\partial \sigma'}\frac{\partial \sigma'}{\partial e}\frac{\partial e}{\partial r}=(-1)\left(-\frac{1}{a_V}\right)\frac{\partial e}{\partial r}=\frac{1}{a_V}\frac{\partial e}{\partial r}. \tag{85}$$

The governing equation can then be represented strictly in terms of the void ratio as

$$\frac{1}{(1+e)^2}\frac{\partial e}{\partial t}=\frac{1}{r}\frac{\partial}{\partial r}\left(D_V(e)\cdot r\frac{\partial e}{\partial r}\right), \tag{86}$$

where the void diffusivity is defined as

$$D_V(e)\equiv\frac{k(e)}{\mu a_V(e)}\frac{1}{1+e}=\frac{D_0\,exp(Ge)}{1+e}. \tag{87}$$

The last term in (87) for the void diffusivity is obtained by assuming exponential dependency for permeability k and a_V, containing the two adjustable parameters D_0 (m^2/s), and G (–), which can be determined by fitting experimental results.

A governing equation to determine the location of extruding bentonite is derived by evaluating the net mass flow rate of water through the boundaries at R_0 and at $R(t)$. The derivation considers the overall rate of change of the mass of water in the domain, as

$$\frac{d}{dt}\left[\rho V_W(t)\right]=\dot{m}_{R_0}+\dot{m}_{R(t)}, \tag{88}$$

where $V_W(t)$ (m^3) is the volume of water, $\dot{m}_{R_0}$ (kg/s) is the mass flow of water at the intersection R_0, and $\dot{m}_{R(t)}$ (kg/s) is the mass flow of water at the tip of expansion $R(t)$, formulated as, using Darcy's law $\underline{q}$ (m/s),

$$\dot{m}_{R(t)} = -\frac{1}{1+e} 2\pi R(t) L\rho\, \underline{q} \cdot \underline{n}\Big|_{R(t)}, \text{ and } \dot{m}_{R_0} = -\frac{1}{1+e} 2\pi R_0 L\rho\, \underline{q} \cdot \underline{n}\Big|_{R_0}. \qquad (89) \text{ and } (90)$$

Fracture aperture is given by L (m). The unit normal vector is shown by $\underline{n}$, indicating the outward direction normal to the boundary. The rate of solid volume flow is obtained in a similar manner. The rate of change of the water volume is expressed as the difference between the rate of change of total volume and the solid volume and combined with Darcy's law (82), and (85), to obtain

$$\frac{d}{dt}\left[R(t)\right] = 2D_V(e)\frac{\partial e}{\partial r}\Big|_{R(t)}. \qquad (91)$$

Conditions for (87) are: $e(r,0) = e_0$, $0 \le r \le R_0$; $e(R_0, t) = e_0$, $t > 0$; $e(R(t),t) = e_T$, $t > 0$. The condition for (91) is: $R(0) = R_0$.

The radionuclide transport is modeled based on the volume averaging concept for a heterogeneous water-solid medium.[22] The model is derived for a single radionuclide. Contribution from the parent radionuclide is not considered. Radionuclide concentration in the fluid phase N_F (g/m^3) is given by

$$\begin{aligned}&\frac{\partial}{\partial t}\left(\varepsilon_F N_F + \sigma K_D N_F\right) + \frac{1}{r}\frac{\partial}{\partial r}\cdot\left(r\cdot\varepsilon_F \underline{v}_F N_F + r\cdot\sigma \underline{v}_S K_D N_F\right) - \frac{1}{r}\frac{\partial}{\partial r}\cdot\left(D_F r\frac{\partial}{\partial r}\left(\varepsilon_F N_F\right)\right), \\ &+\lambda\left(\varepsilon_F N_F + \sigma K_D N_F\right) = 0\end{aligned} \qquad (92)$$

where ε_F (–) is fluid porosity, λ ($1/s$) represents decay, σ (–) is solid volume fraction, D_F (m^2/s) is molecular diffusion coefficient of the radionuclide in water, and K_D (–) is the distribution coefficient, where $K_D = k_D\rho_B$, k_D (cm^3/g) is the sorption distribution coefficient and ρ_B (g/cm^3) is the density of bentonite. At $r = R_S$, the radionuclide concentration is assumed to vanish. The side conditions to the model (92) are given: $N_F(r,0) = 0$, $R_0 \le r \le R_S$; $N_F(R_0,t) = N^*$, $t > 0$; $N_F(R_S,t) = 0$, $t > 0$.

The equation (92) is then transformed into a dimensionless one. Normalized concentration, spatial domain, time domain, Peclet number, and Thiele modulus are defined as

$$N \equiv \frac{N_F}{N^*}, \bar{r} \equiv \frac{r}{R_0}, \quad \bar{R}_T \equiv \frac{R_S}{R_0}, \quad \bar{t} \equiv \frac{D_F t}{R_0^2}, \chi \equiv \frac{\underline{v}_F R_0}{D_F}, \text{ and } \Lambda \equiv \frac{R_0^2 \lambda}{D_F}. \qquad (93)$$

In (92), the derivatives within each term are computed, then (93) is utilized to obtain

$$\bar{\alpha}\frac{\partial N}{\partial \bar{t}}+\bar{\beta}\frac{\partial N}{\partial \bar{r}}-\frac{1}{\bar{r}}\frac{\partial}{\partial \bar{r}}\left[\bar{\gamma}\left(\bar{r}\frac{\partial N}{\partial \bar{r}}\right)\right]+\bar{\theta}N=0. \tag{94}$$

All of the parameters in the model (94) vary with dimensionless space and time. In the region of extruding bentonite, parameters are evaluated in terms of the void ratio distribution obtained from the solution to (86) and (91). The parameters are defined as

$$\bar{\alpha}\equiv\varepsilon_F\left[1+\frac{K_D}{e}\right],\bar{\beta}\equiv\varepsilon_F\chi\left[1+\frac{\sigma\underline{v}_S K_D-D_F\dfrac{\partial\varepsilon_F}{\partial\bar{r}}}{\varepsilon_F\underline{v}_F}\right],\bar{\gamma}\equiv\varepsilon_F, \text{ and } \bar{\theta}\equiv\bar{\alpha}\Lambda+\frac{\bar{\beta}}{\bar{r}}+\frac{\partial\bar{\beta}}{\partial\bar{r}}+\frac{\partial\bar{\alpha}}{\partial\bar{t}}. \tag{95}$$

In the region beyond the extruding tip, the parameters are defined by the physical conditions in the system, $e=\infty$, $\varepsilon_F=1$, $\sigma=0$, and $\underline{v}_S=0$. Fluid velocity is determined by the overall conservation of groundwater in the system. Conditions in the dimensionless model space are: $N(\bar{r},0)=0, 1\le\bar{r}\le\bar{R}_T$; $N(1,\bar{t})=1,\bar{t}>0$; $N(\bar{R}_T,\bar{t})=0,\bar{t}>0$.

Finite element solutions have been obtained for (95). The input data utilized in this numerical simulation in was based on prior, independent experimental data and a modeling simulation.[23]

In Figure 19, the spatial distribution of the radionuclide concentration in the dimensionless model space is shown for various values of sorption distribution (k_D) at $t = 97.3\ h$. Trends are indicative of the overall behavior observed for simulations at: $100\ s < t < 100\ h$. Results indicate that concentration in the fluid phase exceeds source concentration for $k_D \ge 100\ cm^3/g$. With increasing sorption, the migration distance of the radionuclide into the fracture decreases. For $k_D \ge 1700\ cm^3/g$, the radionuclide remains completely contained in the region of bentonite extrusion. The location of the expanding tip is shown in Figure 19.

Near the source (N^*), concentration remains high in the fluid phase. Radionuclides sorb to bentonite, migrate in the outward direction by solid phase advection, and desorb into the water phase, resulting in a peak in the middle of the region of extrusion. With increasing sorption, the retardation factor ($K = 1+K_D/e$) increases, leading to higher values closer to the source. More radionuclides sorb to solid material; however, migration in the fluid phase is also inhibited. Migration distance decreases, more radionuclides are contained within a smaller volume, and fluid phase concentrations increase. These results suggest that residence time in the extrusion region would be significantly long due to the aforementioned transport mechanism. Short lived radionuclides could eventually vanish, due to decay, within this extrusion region. This added barrier to release suggests importance of the region in the vicinity of buffer/rock interface.

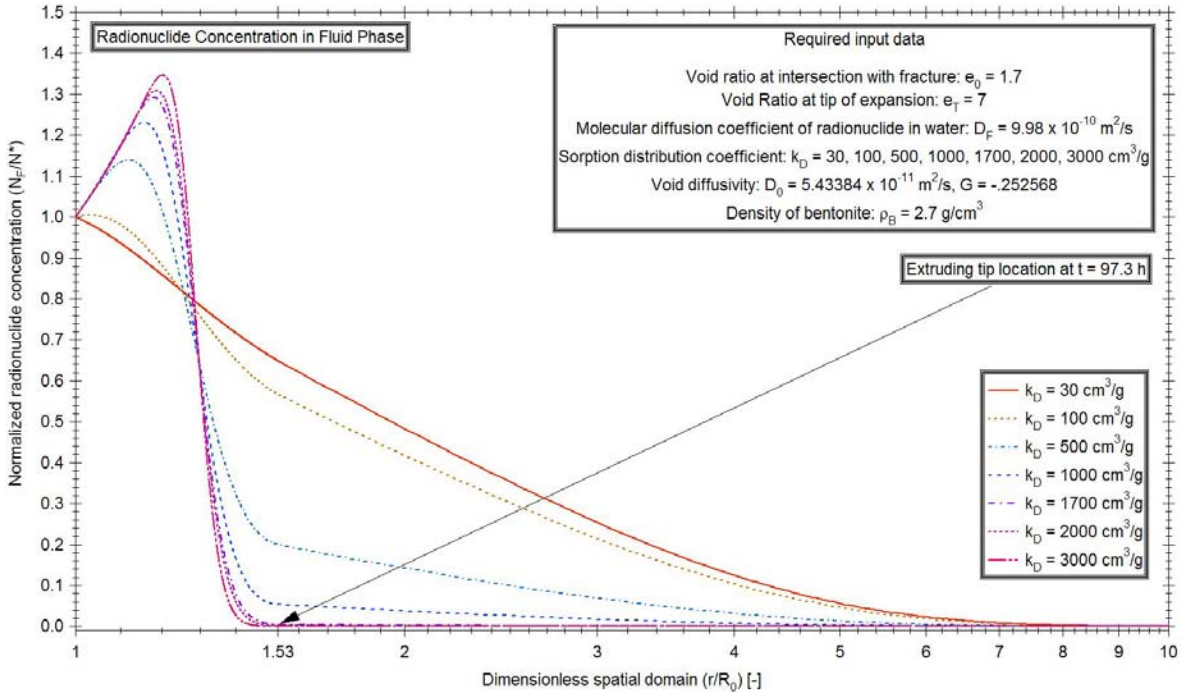

Figure 19: Transport of a strongly sorbing nuclide in the planar fracture with fluid phase advection, solid phase advection, and sorption on moving solid particles.

Results of numerical exploration have revealed that utilization of bentonite as the buffer in the water saturated repository would have favorable effects on the repository performance, in addition to those already recognized in previous studies. Due to bentonite-particle flow in the outward direction, radionuclide residence time could be significantly long, especially with strong sorption. For short lived radionuclides, the transport phenomena observed in this study could significantly decrease the release rate to the exterior region. This indicates that the added barrier between the bentonite-buffer region in the EBS and the near-field host rock could considerably affect repository performance in a favorable manner. Validation of this model can allow for long term analyses and eventual inclusion into future repository performance assessments.

V. Closing remarks

The tasks planned in the agreement have been performed. Analytical formulations for two-phase flow situations in the engineered barrier region have been completed. For numerical evaluations, several codes are available.

Analytical formulations for radionuclide transport have also been considered. Discussions have been made to better understand in which cases this coupling feature should be incorporated in the performance models. So far, understanding is that for radionuclide migration, necessity of coupling T effects is secondary. Nevertheless, efforts have started to make a scoping evaluation for the effects of thermally driven water flow on the radionuclide release from a failed package. After obtaining results of this scoping evaluation, we can make better judgment. Discussions and consultations with KAERI in this area will be greatly useful to make this project more fruitful.

Acknowledgment
The Principal Investigator of the project at UCBNE is grateful for discussions with Dr. Chul Hyung Kang of KAERI, who is currently staying at UCBNE as his sabbatical.

[1] A series of books published by Jacob Bear. For example, Jacob Bear and Yehuda Bachmat, "Introduction to Modeling of Transport Phenomena in Porous Media," Kluwer Academic Publishers, ISBN 0-7923-0557-4.

[2] K. S. Udell, *Int. J. Heat Mass Transfer*, **28**(2), 485 (1985).

[3] P. L. Chambré, T. H. Pigford, A. Fujita, T. Kanki, A. Kobayashi, H. Lung, D. Ting, Y. Sato, and S. J. Zavoshy, Analytical Performance Models for Geologic Repositories, Lawrence Berkeley Laboratory, LBL-14842, Vol. 2 (1982).

[4] K. Pruess, The TOUGH Codes – A Family of Simulation Tools for Multiphase Flow and Transport Processes in Permeable Media, *Vadose Zone Journal*, **3**, 738-746 (2004)

[5] For example, R. Pusch, Borehole sealing with highly compacted Na bentonite. SKBF/KBS Teknisk Rapport 81-09 (1981).

[6] L. BÖRGESSON, Interim report on the laboratory and theoretical work in modeling the drained and undrained behavior of buffer materials, SKB Technical Report 90-45 (1990).

[7] For example, T. Kanno, Y. Iwata and H. Sugino, Modelling of bentonite swelling as solid particle diffusion, Clay Science for Engineering, Adachi and Fukue (eds.), Balkema, Rotterdam, ISBN 90 5809 1579 (2001).

[8] J. Y. Boisson, Study on the possibilities by flowing ground waters on bentonite plugs expanded from borehole into fractures, Proc. NEA/CEC Workshop-Sealing of Radioactive Waste Repositories (1989).

[9] R. A. Borrelli and J. Ahn, Radionuclide Transport in a Water-Saturated Planar Fracture with Bentonite Extrusion, *Nuclear Technology, in press*.

[10] van Genuchten, M. Th., *Soil Science Soc. Am. J.,* **44**, 892-898, 1980.

[11] J. Ahn, S. Nagasaki, S. Tanaka, and A. Suzuki, Effects of Smectite Illitization of Transport of Actinides Through Engineered Barriers of HLW Repositories, 18th International Symposium on the Scientific Basis for Nuclear Waste Management, Materials Research Society, Atomic Energy Society of Japan, October 1994, Kyoto, Japan, 1995.

[12] Nagasaki, S., J. Ahn, S. Tanaka, and A. Suzuki, Sorption Behavior of Np(IV), Np(V), and Am(III) in the Disturbed Zone Between Engineered and Natural Barriers, *J. Radioanal. Nucl. Chem., Letters*, **214**(5), 381-389 (1996)

[13] S. P. Altaner, *Geochemica et Cosmochimica Acta*, **53**, 923 (1989).

[14] P. L. Chambré, C. H. Kang, and T. H. Pigford, *Trans. Am. Nuc. Soc.,* **52**, 77 (1986).

[15] T. Ohe, M. Tsukamoto, M. Kinoshita, and T. Inoue, *Waste Management*, **11**, 191 (1991).

[16] S. Nagasaki, J. Ahn, S. Tanaka, and A. Suzuki, Sorption Behavior of Np(IV), Np(V), and Am(III) in the Disturbed Zone Between Engineered and Natural Barriers, *J. Radioanal. Nucl. Chem., Letters*, **214**(5), 381-389 (1996)

[17] J. Ahn and A. Suzuki, Diffusion of the ^{241}Am—> ^{237}Np Decay Chain Limited by Their Elemental Solubilities in Artificial Barriers of High-Level Radioactive Waste Repositories, *Nuclear Technology*, **101**(1), 79—91, 1993.

[18] J. Verbeke, J. Ahn, and P. L. Chambré, "Long-Term Behavior of Buffer Materials in HLW Geologic Repositories," *Proc., 8th International Conf., High-Level Radioactive Waste Management,* Las Vegas, Nevada, American Nuclear Society, (1998).

[19] R. A. Borrelli, R. A. and J. Ahn, "Bentonite Extrusion in Planar Fracture Based on Net Water Flow," *Proc., International Conf., High – Level Radioactive Waste Management,* Las Vegas, Nevada, American Nuclear Society (2006).

[20] G. Gambolati, G. *Water Resources Research,* **9**(5), 1385 – 1395 (1973).

[21] K. Terzaghi, *Colloid Chemistry,* **3**, 65 – 88, (1931).

[22] M. Harada, *et al.*, *Migration of Radionuclides through Sorbing Media: Analytical Solutions – I,* Lawrence Berkeley Laboratory, Earth Sciences Division, Berkeley, CA, (1980).

[23] T. Kanno, T. and Y. Iwata, *Study on Model for Bentonite Buffer Intrusion (II),* JNC, Japan, (2003).